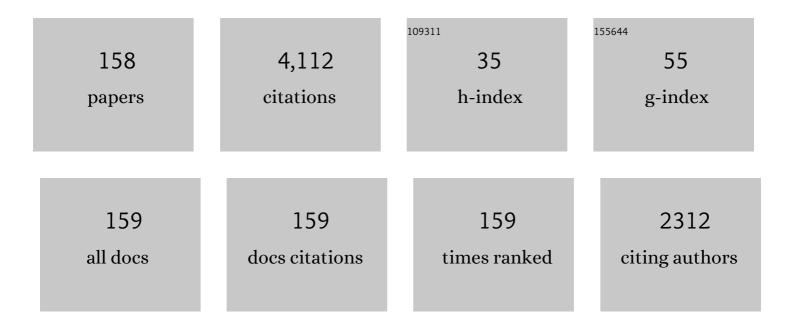
Xi-Tao Wang

List of Publications by Year in descending order

Source: https://exaly.com/author-pdf/2939998/publications.pdf Version: 2024-02-01



#	Article	IF	CITATIONS
1	Enhanced thermal conductivity in copper matrix composites reinforced with titanium-coated diamond particles. Scripta Materialia, 2011, 65, 1097-1100.	5.2	212
2	A comparative study on Johnson–Cook, modified Johnson–Cook and Arrhenius-type constitutive models to predict the high temperature flow stress in 20CrMo alloy steel. Materials & Design, 2013, 52, 677-685.	5.1	199
3	High thermal conductivity through interfacial layer optimization in diamond particles dispersed Zr-alloyed Cu matrix composites. Scripta Materialia, 2015, 109, 72-75.	5.2	136
4	Effect of Ti interlayer on interfacial thermal conductance between CuÂand diamond. Acta Materialia, 2018, 160, 235-246.	7.9	111
5	Microstructure and thermal conductivity of Cu/diamond composites with Ti-coated diamond particles produced by gas pressure infiltration. Journal of Alloys and Compounds, 2015, 647, 941-946.	5.5	95
6	Mechanical and thermal properties of carbon nanotube/aluminum composites consolidated by spark plasma sintering. Materials & Design, 2012, 41, 344-348.	5.1	91
7	Microstructure evolution and impact fracture behaviors of Z3CN20-09M stainless steels after long-term thermal aging. Journal of Nuclear Materials, 2013, 433, 41-49.	2.7	86
8	Effects of ion irradiation on microstructure and properties of zirconium alloys—A review. Nuclear Engineering and Technology, 2015, 47, 323-331.	2.3	81
9	Optimized thermal properties in diamond particles reinforced copper-titanium matrix composites produced by gas pressure infiltration. Composites Part A: Applied Science and Manufacturing, 2016, 91, 189-194.	7.6	80
10	Enhanced thermal conductivity in Cu/diamond composites by tailoring the thickness of interfacial TiC layer. Composites Part A: Applied Science and Manufacturing, 2018, 113, 76-82.	7.6	80
11	Combining Cr pre-coating and Cr alloying to improve the thermal conductivity of diamond particles reinforced Cu matrix composites. Journal of Alloys and Compounds, 2018, 749, 1098-1105.	5.5	78
12	High thermal conductivity of Cu-B/diamond composites prepared by gas pressure infiltration. Journal of Alloys and Compounds, 2018, 735, 1648-1653.	5.5	75
13	G-phase precipitation in duplex stainless steels after long-term thermal aging: A high-resolution transmission electron microscopy study. Journal of Nuclear Materials, 2014, 452, 382-388.	2.7	73
14	Annealing induced recovery of long-term thermal aging embrittlement in a duplex stainless steel. Materials Science & Engineering A: Structural Materials: Properties, Microstructure and Processing, 2013, 564, 85-91.	5.6	68
15	Thermal conductivity of Cu–Zr/diamond composites produced by high temperature–high pressure method. Composites Part B: Engineering, 2015, 68, 22-26.	12.0	67
16	Microstructures and mechanical properties of cast austenite stainless steels after long-term thermal aging at low temperature. Materials & Design, 2013, 50, 886-892.	5.1	66
17	Tailoring interface structure and enhancing thermal conductivity of Cu/diamond composites by alloying boron to the Cu matrix. Materials Characterization, 2019, 152, 265-275.	4.4	66
18	Effect of copper content on the thermal conductivity and thermal expansion of Al–Cu/diamond composites. Materials & Design, 2012, 39, 87-92.	5.1	65

#	Article	IF	CITATIONS
19	Investigation on the 1000, 1150 and 1400 °C isothermal section of the Tiî—,Alî—,Nb system. Intermetallics, 1996, 4, 13-22.	3.9	63
20	A modified Zerilli–Armstrong constitutive model to predict hot deformation behavior of 20CrMo alloy steel. Materials & Design, 2014, 56, 122-127.	5.1	57
21	A physically-based constitutive model for a nitrogen alloyed ultralow carbon stainless steel. Computational Materials Science, 2015, 98, 64-69.	3.0	56
22	Interfacial structure evolution of Ti-coated diamond particle reinforced Al matrix composite produced by gas pressure infiltration. Composites Part B: Engineering, 2017, 113, 285-290.	12.0	56
23	Effect of sigma phase precipitation on the mechanical and wear properties of Z3CN20.09M cast duplex stainless steel. Nuclear Engineering and Design, 2013, 259, 1-7.	1.7	50
24	Interfacial structure evolution and thermal conductivity of Cu-Zr/diamond composites prepared by gas pressure infiltration. Journal of Alloys and Compounds, 2019, 781, 800-809.	5.5	50
25	Non-uniform phase separation in ferrite of a duplex stainless steel. Acta Materialia, 2017, 140, 388-397.	7.9	49
26	Nucleation and growth mechanisms of interfacial Al 4 C 3 in Al/diamond composites. Journal of Alloys and Compounds, 2016, 657, 81-89.	5.5	46
27	Effects of Co additions on electromigration behaviors in Sn–3.0ÂAg–0.5ÂCu-based solder joint. Journal of Materials Science, 2011, 46, 4896-4905.	3.7	44
28	Grain morphology and crystal structure of pre-transition oxides formed on Zircaloy-4. Corrosion Science, 2013, 74, 323-331.	6.6	44
29	The role of alloying elements in the initiation of nanoscale porosity in oxide films formed on zirconium alloys. Corrosion Science, 2013, 77, 391-396.	6.6	43
30	Regulated Interfacial Thermal Conductance between Cu and Diamond by a TiC Interlayer for Thermal Management Applications. ACS Applied Materials & Interfaces, 2019, 11, 26507-26517.	8.0	41
31	Optimisation of high thermal conductivity Al/diamond composites produced by gas pressure infiltration by controlling infiltration temperature and pressure. Journal of Materials Science, 2015, 50, 688-696.	3.7	40
32	Microstructure, Mechanical Properties and InÂVitro Degradation Behavior of a Novel Biodegradable Mg–1.5Zn–0.6Zr–0.2Sc Alloy. Journal of Materials Science and Technology, 2015, 31, 744-750.	10.7	38
33	Effect of metalloid silicon addition on densification, microstructure and thermal–physical properties of Al/diamond composites consolidated by spark plasma sintering. Materials & Design, 2014, 63, 838-847.	5.1	37
34	Effects of ferrite content on the mechanical properties of thermal aged duplex stainless steels. Materials Science & Engineering A: Structural Materials: Properties, Microstructure and Processing, 2015, 625, 186-193.	5.6	37
35	Mechanical properties of diamond/Al composites with Ti-coated diamond particles produced by gas-assisted pressure infiltration. Materials Science & Engineering A: Structural Materials: Properties, Microstructure and Processing, 2015, 626, 362-368.	5.6	36
36	Interfacial characteristic and thermal conductivity of Al/diamond composites produced by gas pressure infiltration in a nitrogen atmosphere. Materials and Design, 2016, 92, 643-648.	7.0	36

#	Article	IF	CITATIONS
37	Microstructural evolution in 316LN austenitic stainless steel during solidification process under different cooling rates. Journal of Materials Science, 2016, 51, 2529-2539.	3.7	36
38	Evolution of the microstructure in aged G115 steels with the different concentration of tungsten. Materials Science & Engineering A: Structural Materials: Properties, Microstructure and Processing, 2018, 729, 161-169.	5.6	36
39	Electromigration in Sn-Bi Modified with Polyhedral Oligomeric Silsesquioxane. Journal of Electronic Materials, 2010, 39, 2513-2521.	2.2	35
40	Retarding the electromigration effects to the eutectic SnBi solder joints by micro-sized Ni-particles reinforcement approach. Journal of Alloys and Compounds, 2011, 509, 878-884.	5.5	34
41	Modified arrhenius-type constitutive model and artificial neural network-based model for constitutive relationship of 316LN stainless steel during hot deformation. Journal of Iron and Steel Research International, 2015, 22, 721-729.	2.8	34
42	Evaluation of hardening behaviors in ion-irradiated Fe–9Cr and Fe–20Cr alloys by nanoindentation technique. Journal of Nuclear Materials, 2016, 478, 50-55.	2.7	34
43	Experimental and theoretical characterization of electrical contact in anisotropically conductive adhesive. IEEE Transactions on Advanced Packaging, 2000, 23, 15-21.	1.6	33
44	The coupling effects of thermal cycling and high current density on Sn58Bi solder joints. Journal of Materials Science, 2013, 48, 2318-2325.	3.7	33
45	Effect of boron addition on interface microstructure and thermal conductivity of Cu/diamond composites produced by high temperature–high pressure method. Physica Status Solidi (A) Applications and Materials Science, 2014, 211, 587-594.	1.8	33
46	The role of Ti coating in enhancing tensile strength of Al/diamond composites. Materials Science & Engineering A: Structural Materials: Properties, Microstructure and Processing, 2013, 565, 33-37.	5.6	32
47	The role of Cr interlayer in determining interfacial thermal conductance between Cu and diamond. Applied Surface Science, 2020, 515, 146046.	6.1	32
48	The formation of atomic-level interfacial layer and its effect on thermal conductivity of W-coated diamond particles reinforced Al matrix composites. Composites Part A: Applied Science and Manufacturing, 2018, 107, 164-170.	7.6	29
49	Positron annihilation study of proton-irradiated reactor pressure vessel steels. Radiation Physics and Chemistry, 2012, 81, 1586-1592.	2.8	28
50	Interfacial products and thermal conductivity of diamond/Al composites reinforced with ZrC-coated diamond particles. Diamond and Related Materials, 2019, 100, 107565.	3.9	28
51	Effects of electromigration on resistance changes in eutectic SnBi solder joints. Journal of Materials Science, 2011, 46, 3544-3549.	3.7	27
52	Effects of scandium addition on biocompatibility of biodegradable Mg–1.5Zn–0.6Zr alloy. Materials Letters, 2018, 215, 200-202.	2.6	27
53	Investigation of the microstructure and strength in G115 steel with the different concentration of tungsten during creep test. Materials Characterization, 2019, 149, 95-104.	4.4	27
54	Effect of Metal Matrix Alloying on Mechanical Strength of Diamond Particle-Reinforced Aluminum Composites. Journal of Materials Engineering and Performance, 2015, 24, 2556-2562.	2.5	26

#	Article	IF	CITATIONS
55	The failure models of Sn-based solder joints under coupling effects of electromigration and thermal cycling. Journal of Applied Physics, 2013, 113, .	2.5	25
56	Microstructure, mechanical property and inÂvitro biocorrosion behavior of single-phase biodegradable Mg–1.5Zn–0.6Zr alloy. Journal of Magnesium and Alloys, 2014, 2, 181-189.	11.9	25
57	Influence of albumin on in vitro degradation behavior of biodegradable Mg-1.5Zn-0.6Zr-0.2Sc alloy. Materials Letters, 2018, 217, 227-230.	2.6	25
58	Effect of boron on G115 martensitic heat resistant steel during aging at 650°C. Materials Science & Engineering A: Structural Materials: Properties, Microstructure and Processing, 2020, 787, 139529.	5.6	25
59	Reinforcement size effect on thermal conductivity in Cu-B/diamond composite. Journal of Materials Science and Technology, 2021, 91, 1-4.	10.7	25
60	Effect of diamond surface chemistry and structure on the interfacial microstructure and properties of Al/diamond composites. RSC Advances, 2016, 6, 67252-67259.	3.6	24
61	Effect of Zr Content on Mechanical Properties of Diamond/Cu-Zr Composites Produced by Gas Pressure Infiltration. Journal of Materials Engineering and Performance, 2018, 27, 714-720.	2.5	21
62	Thermo-Physical Properties of Ti-Coated Diamond/Al Composites Prepared by Pressure Infiltration. Materials Science Forum, 2010, 654-656, 2572-2575.	0.3	20
63	Effects of long-term thermal aging on the stress corrosion cracking behavior of cast austenitic stainless steels in simulated PWR primary water. Journal of Nuclear Materials, 2016, 469, 262-268.	2.7	20
64	Partial phase diagram of the Ti-Al binary system. Journal of Phase Equilibria and Diffusion, 1996, 17, 117-120.	0.3	19
65	Strengthening of σ phase in a Fe20Cr9Ni cast austenite stainless steel. Materials Characterization, 2013, 84, 120-125.	4.4	19
66	The 1400°C isothermal section of the Ti-Al-Nb ternary system. Journal of Phase Equilibria and Diffusion, 1998, 19, 200-205.	0.3	18
67	Electrical characterization of isotropic conductive adhesive under mechanical loading. Journal of Electronic Materials, 2002, 31, 916-920.	2.2	18
68	Investigation of hardening behavior in Xe ion-irradiated Zr–1Nb. Journal of Nuclear Materials, 2016, 473, 256-263.	2.7	18
69	Effect of Precipitated Phases on the Pitting Corrosion of Z3CN20.09M Cast Duplex Stainless Steel. Materials Transactions, 2013, 54, 839-843.	1.2	17
70	Effect of Xe26+ ion irradiation on the microstructural evolution and mechanical properties of Zr–1Nb at room and high temperature. Journal of Nuclear Materials, 2015, 461, 78-84.	2.7	17
71	Recrystallization behavior of cold-rolled Zr–1Nb alloy. Journal of Nuclear Materials, 2015, 456, 321-328.	2.7	17
72	Mo-interlayer-mediated thermal conductance at Cu/diamond interface measured by time-domain thermoreflectance. Composites Part A: Applied Science and Manufacturing, 2020, 135, 105921.	7.6	17

#	Article	IF	CITATIONS
73	Unveiling interfacial structure and improving thermal conductivity of Cu/diamond composites reinforced with Zr-coated diamond particles. Vacuum, 2022, 202, 111133.	3.5	17
74	Probabilistic fracture mechanics analysis of thermally aged nuclear piping in a pressurized water reactor. Nuclear Engineering and Design, 2013, 265, 611-618.	1.7	16
75	Tunable coefficient of thermal expansion of Cu-B/diamond composites prepared by gas pressure infiltration. Journal of Alloys and Compounds, 2019, 794, 473-481.	5.5	16
76	Formation behavior of long needle-like M23C6 carbides in a nickel-based alloy without γ' phase during long time aging. Journal of Alloys and Compounds, 2020, 821, 153259.	5.5	16
77	Quantitative estimate of the characteristics of conductive particles in ACA by using nano-indenter. IEEE Transactions on Components and Packaging Technologies, 1998, 21, 248-251.	0.7	15
78	Effects of prior solution treatment on thermal aging behavior of duplex stainless steels. Journal of Nuclear Materials, 2013, 441, 337-342.	2.7	15
79	Tensile behaviour of 316LN stainless steel at elevated temperatures. Materials at High Temperatures, 2014, 31, 198-203.	1.0	15
80	Effects of Ni content on the microstructures, mechanical properties and thermal aging embrittlement behaviors of Fe–20Cr–xNi alloys. Materials Science & Engineering A: Structural Materials: Properties, Microstructure and Processing, 2015, 639, 640-646.	5.6	15
81	Phase-field simulation of multi-phase interactions in Fe-C peritectic solidification. Computational Materials Science, 2020, 171, 109220.	3.0	15
82	Carbide dissolution and grain growth behavior of a nickel-based alloy without γ′ phase during solid solution. Journal of Alloys and Compounds, 2020, 825, 154106.	5.5	15
83	Reply to the "comment on â€~investigation on the 1000, 1150 and 1400 °C isothermal section of the Tiî—,Alî system'â€â€"Part I. Ordering of Nb in γ-TiAl and γ1 phase. Intermetallics, 1998, 6, 323-327.	– <u>.</u> Np	14
84	Proton-irradiation-induced damage in Fe–0.3wt.%Cu alloys characterized by positron annihilation and nanoindentation. Nuclear Instruments & Methods in Physics Research B, 2013, 307, 545-551.	1.4	14
85	Aluminum carbide hydrolysis induced degradation of thermal conductivity and tensile strength in diamond/aluminum composite. Journal of Composite Materials, 2018, 52, 2709-2717.	2.4	14
86	Effects of scandium addition on the in vitro degradation behavior of biodegradable Mg–1.5Zn–0.6Zr alloy. Journal of Materials Science, 2018, 53, 14075-14086.	3.7	14
87	Interface characterization of a Cu–Ti-coated diamond system. Surface and Coatings Technology, 2015, 278, 163-170.	4.8	13
88	A brittle fracture mechanism in thermally aged duplex stainless steels revealed by in situ high-energy X-ray diffraction. Materials Science & Engineering A: Structural Materials: Properties, Microstructure and Processing, 2019, 739, 264-271.	5.6	13
89	Study of Static Recrystallization Behavior of a Nitrogen-Alloyed Ultralow Carbon Austenitic Stainless Steel by Experiment and Simulation. Journal of Materials Engineering and Performance, 2015, 24, 4346-4357.	2.5	12
90	Hot deformation behavior of a heat-resistant alloy without γ′-phase. Journal of Iron and Steel Research International, 2020, 27, 820-833.	2.8	12

#	Article	IF	CITATIONS
91	Improved wear resistance of biodegradable Mg–1.5Zn–0.6Zr alloy by Sc addition. Rare Metals, 2021, 40, 2206-2212.	7.1	12
92	Calculation of Jackson's factor of Mg2Si in Mg melt using coordination polyhedron. Journal of Alloys and Compounds, 2013, 581, 494-497.	5.5	11
93	Effect of milling duration on hydrogen storage thermodynamics and kinetics of ball-milled Ce–Mg–Ni-based alloy powders. Journal of Iron and Steel Research International, 2018, 25, 746-754.	2.8	11
94	Phase-field model of graphene aerogel formation by ice template method. Applied Physics Letters, 2019, 115, 111901.	3.3	11
95	In Situ Observation of the Deformation and Fracture Behaviors of Long-Term Thermally Aged Cast Duplex Stainless Steels. Metals, 2019, 9, 258.	2.3	11
96	The influence of silicon content on the thermal conductivity of Al-Si/diamond composites. , 2009, , .		10
97	Effects of long term thermal aging on high temperature tensile deformation behaviours of duplex stainless steels. Materials at High Temperatures, 2015, 32, 524-529.	1.0	10
98	Effects of Ball Milling Processing Conditions and Alloy Components on the Synthesis of Cu-Nb and Cu-Mo Alloys. Materials, 2019, 12, 1224.	2.9	10
99	Creep behaviour of a novel CoNi-base single-crystal superalloy at high temperature and low stress. Materials Letters, 2020, 262, 127042.	2.6	10
100	Improved corrosion resistance of Mg alloy by a green phosphating: insights into pre-activation, temperature, and growth mechanism. Journal of Materials Science, 2021, 56, 828-843.	3.7	10
101	Effect of thermal aging on the mechanical, intergranular corrosion and corrosion fatigue properties of Z3CN20.09M cast duplex stainless steel. Nuclear Engineering and Technology, 2021, 53, 2591-2599.	2.3	10
102	Hot-Rolled TRIP Steels Based on Dynamic Transformation of Undercooled Austenite. Materials Science Forum, 0, 654-656, 250-253.	0.3	9
103	Effect of thermal aging on the fatigue crack growth behavior of cast duplex stainless steels. International Journal of Minerals, Metallurgy and Materials, 2015, 22, 1163-1170.	4.9	9
104	Investigation of ion irradiation hardening behaviors of tempered and long-term thermal aged T92 steel. Journal of Nuclear Materials, 2018, 511, 191-199.	2.7	9
105	Investigation of Stress Evolution Induced by Electromigration in Sn-Ag-Cu Solder Joints Based on an X-Ray Diffraction Technique. Journal of Electronic Materials, 2012, 41, 425-430.	2.2	8
106	Enhanced mechanical properties in Al/diamond composites by Si addition. Rare Metals, 2016, 35, 701-704.	7.1	8
107	Multiphase-field approach with parabolic approximation scheme. Computational Materials Science, 2020, 172, 109322.	3.0	8
108	Fe-C peritectic solidification of polycrystalline ferrite by phase-field method. Computational Materials Science, 2020, 178, 109626.	3.0	8

#	Article	IF	CITATIONS
109	Microstructural evolution of sandwiched Cr interlayer in Cu/Cr/diamond subjected to heat treatment. Thin Solid Films, 2021, 736, 138911.	1.8	8
110	PRECIPITATION BEHAVIOR OF THE INTERMETALLIC PHASES IN Z3CN20.09M STAINLESS STEEL FOR PRIMARY COOLANT PIPES OF NUCLEAR POWER PLANT. Jinshu Xuebao/Acta Metallurgica Sinica, 2013, 49, 415.	0.3	8
111	Effect of yttrium addition on microstructure and orientation of hydride precipitation in Zr-1Nb alloy. International Journal of Hydrogen Energy, 2014, 39, 21116-21126.	7.1	7
112	Effect of thermal aging on the leak-before-break analysis of nuclear primary pipes. Nuclear Engineering and Design, 2014, 280, 493-500.	1.7	7
113	Influence of Initial Microstructures on Deformation Behavior of 316LN Austenitic Steels at 400-900°C. Journal of Materials Engineering and Performance, 2015, 24, 694-699.	2.5	7
114	Highly ameliorated gaseous and electrochemical hydrogen storage dynamics of nanocrystalline and amorphous LaMg12-type alloys prepared by mechanical milling. Journal of Iron and Steel Research International, 2017, 24, 50-58.	2.8	7
115	Nano-Deformation Behavior of a Thermally Aged Duplex Stainless Steel Investigated by Nanoindentation, FIB and TEM. Journal of Materials Engineering and Performance, 2018, 27, 4714-4721.	2.5	7
116	Microstructure and creep strength evolution in G115 steel during creep at 650 °C. Materials Research Express, 2020, 7, 016528.	1.6	7
117	Mechanical Properties of Cu-B/Diamond Composites Prepared by Gas Pressure Infiltration. Journal of Materials Engineering and Performance, 2020, 29, 3107-3119.	2.5	7
118	Effects of thermal aging temperature and Cr content on phase separation kinetics in Fe-Cr alloys simulated by the phase field method. International Journal of Minerals, Metallurgy and Materials, 2013, 20, 1067-1075.	4.9	6
119	Flow Behavior Modeling of a Nitrogen-Alloyed Ultralow Carbon Stainless Steel During Hot Deformation: A Comparative Study of Constitutive Models. Journal of Materials Engineering and Performance, 2015, 24, 4106-4118.	2.5	6
120	Characterization of Impact Deformation Behavior of a Thermally Aged Duplex Stainless Steel by EBSD. Acta Metallurgica Sinica (English Letters), 2018, 31, 798-806.	2.9	6
121	Effect of tempering temperatures on microstructures and properties of 0.28C–0.22Ti wear-resistant steel. Materials Science and Technology, 2018, 34, 86-94.	1.6	6
122	Microstructure and mechanical property of biodegradable Mg–1.5Zn–0.6Zr alloy with varying contents of scandium. Materials Letters, 2018, 229, 60-63.	2.6	6
123	Comparison of the effects of pre-activators on morphology and corrosion resistance of phosphate conversion coating on magnesium alloy. Journal of Magnesium and Alloys, 2021, , .	11.9	6
124	EFFECT OF LONG TERM AGING ON THE MICROSTRUC-TURE AND MECHANICAL PROPERTIES OF CAST AUSTENITIC STAINLESS STEELS. Jinshu Xuebao/Acta Metallurgica Sinica, 2011, 46, 1186-1191.	0.3	6
125	Effect of Graphite Content on the Conductivity, Wear Behavior, and Corrosion Resistance of the Organic Layer on Magnesium Alloy MAO Coatings. Coatings, 2022, 12, 434.	2.6	6
126	Microstructural modelling of dynamic recrystallisation in Nb microalloyed steels. Materials Science and Technology, 2012, 28, 778-782.	1.6	5

#	Article	IF	CITATIONS
127	Effect of cooling rate on microstructure, hardness, and residual stress of 0.28C–0.22Ti wear-resistant steel. Journal of Iron and Steel Research International, 2019, 26, 866-874.	2.8	5
128	Effects of Tempering Temperature on the Microstructure and Mechanical Properties of T92 Heat-Resistant Steel. Metals, 2019, 9, 194.	2.3	5
129	Proton irradiation induced defects in T92 steels: An investigation by TEM and positron annihilation spectroscopy. Nuclear Instruments & Methods in Physics Research B, 2019, 442, 59-66.	1.4	5
130	The Pitting Corrosion Behavior of the Austenitic Stainless Steel 308L-316L Welded Joint. Metals, 2020, 10, 1258.	2.3	5
131	On the temperature-dependent diffusion growth of ï⊷Mg5Al2Zn2 ternary intermetallic compound in the Mg–Al–Zn system. Journal of Materials Science, 2021, 56, 3488-3497.	3.7	5
132	Corrosion behavior of Zr–Nb–Cr cladding alloys. Rare Metals, 2013, 32, 480-485.	7.1	4
133	A physically based dynamic recrystallization model considering orientation effects for a nitrogen alloyed ultralow carbon stainless steel during hot forging. Journal of Iron and Steel Research International, 2016, 23, 364-371.	2.8	4
134	Microstructure and properties of 1100ÂMPa grade low-carbon hot-rolled steel by laser welding. Journal of Iron and Steel Research International, 2018, 25, 228-234.	2.8	4
135	Influence of Mo Additions on the Mechanical Properties of Cast Duplex Stainless Steels before and after Thermal Aging. Metals, 2019, 9, 295.	2.3	4
136	MICROSTRUCTURE CONTROL OF HOT ROLLED TRIP STEEL BASED ON DYNAMIC TRANSFORMATION OF UNDERCOOLED AUSTENITE I. Prior Austenite Grain Size. Jinshu Xuebao/Acta Metallurgica Sinica, 2010, 2010, 155-160.	0.3	4
137	Retarding electromigration on the Sn-Ag-Cu solder joints by micro-sized metal-particle reinforcement. , 2011, , .		3
138	Leak-before-break analysis of thermally aged nuclear pipe under different bending moments. Nuclear Engineering and Technology, 2015, 47, 712-718.	2.3	3
139	Characterization of Plastic Deformation Behavior of a Thermally Aged Duplex Stainless Steel. Journal of Materials Engineering and Performance, 2017, 26, 2814-2825.	2.5	3
140	The microstructural evolution and mechanical property in G115 steels during long-term aging at 650 °C. Materials Research Express, 2019, 6, 116527.	1.6	3
141	Effects of Thermal Aging on the Low Cycle Fatigue Behaviors of Cast Duplex Stainless Steels. Metals, 2019, 9, 378.	2.3	3
142	Heat transfer in high density electronics packaging. Central South University, 2001, 8, 278-282.	0.5	2
143	MICROSTRUCTURE CONTROL OF HOT ROLLED TRIP STEEL BASED ON DYNAMIC TRANSFORMATION OF UNDERCOOLED AUSTENITE II. Cooling Rate After Dynamic Transformation of Undercooled Austenite. Jinshu Xuebao/Acta Metallurgica Sinica, 2010, 2010, 161-166.	0.3	2
144	Influence of manufacturing processes on Î ² -phase precipitates and corrosion properties of Zr-1Nb alloys. Journal of Nuclear Materials, 2022, 567, 153831.	2.7	2

#	Article	IF	CITATIONS
145	Recent Work on Environmental Embrittlement in Silicides. Materials Research Society Symposia Proceedings, 1996, 460, 575.	0.1	1
146	Implementation of the Internet course on conductive adhesives for electronics packaging. , 0, , .		1
147	Properties of two new medium temperature solders. Soldering and Surface Mount Technology, 2009, 21, 4-8.	1.5	1
148	Microstructural Evolution of Rheo-Diecast AZ91D Magnesium Alloy with Gadolinium Addition. Materials Science Forum, 2010, 654-656, 667-670.	0.3	1
149	Thermal Aging Embrittlement Evaluation of Nuclear Primary Pipe Steel by Ductile to Brittle Transition Test. Advanced Materials Research, 2010, 97-101, 797-800.	0.3	1
150	A Method to Prepare TEM Specimens by Focused Ion Beam Milling for Cu/diamond Composites. Microscopy and Microanalysis, 2018, 24, 838-839.	0.4	1
151	Development of an Internet course on electrically conductive adhesives with experiments. , 0, , .		0
152	Thermal Aging of Primary Circuit Piping Materials in PWR Nuclear Power Plant. Materials Research Society Symposia Proceedings, 2009, 1215, 1.	0.1	0
153	Hot Tensile Deformation and Fracture Behavior of a Nitrogen Alloyed Ultralow Carbon Austenitic Stainless Steel. Materials Transactions, 2015, 56, 1984-1991.	1.2	0
154	Interface tailoring and thermal conductivity enhancement in diamond particles reinforced metal matrix composites. , 2020, , 473-493.		0
155	Evaluation of Thermal Aging Embrittlement in Main Coolant Pipe Steel by Small Punch Test. , 2010, , .		0
156	THE MICROSTRUCTURE AND TENSILE FRACTURE BEHAVIOR OF LONG TERM THERMAL AGED Z3CN20-09M STAINLESS STEEL. Jinshu Xuebao/Acta Metallurgica Sinica, 2013, 49, 175.	0.3	0
157	Study on LBB Behavior of Nuclear Primary Pipes After Long-Term Thermal Aging. , 2014, , 501-508.		0
158	Experimental Investigation and Thermodynamic Verification for the Phase Relation around the ε-Mg23 (Al, Zn)30 Intermetallic Compound in the Mg-Zn-Al System. Materials, 2021, 14, 6892.	2.9	0